Cement and Concrete Research 119 (2019) 21–35

Contents lists available at ScienceDirect

Cement and Concrete Research

journal homepage: www.elsevier.com/locate/cemconres

Thermodynamic modelling of BFS-PC cements under temperature conditions relevant to the geological disposal of nuclear wastes

Dale P. Prentice[a], Brant Walkley[a], Susan A. Bernal[a,b,*], Mark Bankhead[c], Martin Hayes[c], John L. Provis[a,*]

[a] Department of Materials Science and Engineering, The University of Sheffield, Sheffield S1 3JD, UK
[b] School of Civil Engineering, University of Leeds, Woodhouse Lane, Leeds LS2 9JT, UK
[c] National Nuclear Laboratory, Chadwick House, Warrington Road, Birchwood Park, Warrington WA3 6AE, UK

A B S T R A C T

Intermediate level waste produced in UK nuclear power generation is encapsulated or immobilised in blended cements comprising blast furnace slag (BFS) and Portland cement (PC), to be emplaced in a proposed geological disposal facility (GDF). The wasteforms are expected to be exposed to temperatures from 35 to 80 °C during the initial 150 years of GDF operation. Thermodynamic modelling is applied here to describe the phase assemblages of hydrated 1:1, 3:1 and 9:1 BFS-PC blends, with the participation of hydrogarnet as an important phase above 60 °C. The chemical composition of the main phase forming in these systems, an aluminium rich calcium silicate hydrate (C-A-S-H), was well described by a solid-solution model with explicit Al incorporation, although the Al/Si ratio was systematically slightly under-predicted. The developed thermodynamic model predicts the correct phase assemblage across varying temperature regimes, making it a valuable tool to assess the effects of temperature on cements.

1. Introduction

Nuclear power has been used as an energy source across Europe for approximately 70 years, and in the United Kingdom alone, approximately 146,520 m^3 of radioactive waste has been produced as of 2016 [1]. Of this, 110,000 m^3 will require processing and storing in a secure facility. As in many countries, the current policy to manage today's and future nuclear waste in England and Wales is to store it within a geological disposal facility (GDF) [2]. This facility would be the heart of a multi-barrier defence system to ensure that nuclear waste is stored safely and away from the biosphere. The GDF will be a subterranean facility, up to 1 km below the ground, with vaults to store intermediate level waste (ILW) and high level waste (HLW). When these vaults are filled to capacity they will be sealed by Nirex Reference Vault Backfill (NRVB) [3,4], a cementitious high-pH engineered material, to further reduce any transport of radionuclides from the vaults.

To date, UK ILW has been encapsulated in blended cements, primarily Portland Cement (PC) blended with blast furnace slag (BFS). BFS-PC cements have desirable properties for treating nuclear fuel cycle wastes [5–11]:

- The blended cement creates a highly durable, affordable wasteform to store and transport the waste [10];
- High pH of the pore solution (≥12) reduces radionuclide solubility [7–9];
- Cementitious hydration products create high surface area and binding sites for the sorption and/or ionic substitution of radionuclides [7,8];
- Blending PC with high volumes of BFS gives a lower heat of hydration at early age, to avoid excessive temperature rises that may be detrimental to stability [11];
- Stability at varying temperature ranges ensures good durability in a changing temperature environment [11].

The required lifespan of a UK GDF remains to be defined, and a location has not yet been selected. However, an approximate temperature profile has been created to enable scientific work to support a safety case, considering the possible extremes in the conditions to which the cement wasteforms may be exposed (Table 1) [12–15].

1.1. Temperature profile of cemented wasteforms in the GDF

UK ILW waste packages are currently stored above ground at locations across the UK. An average expected temperature of 20 °C has been assumed for this period based on the storage locations [12–15]. Thermal modelling conducted by the Nuclear Decommissioning Authority (NDA) created an extreme case scenario based on the possible heat output of ILW waste packages stored in underground vaults

* Corresponding authors.
E-mail addresses: S.A.BernalLopez@Leeds.ac.uk (S.A. Bernal), j.provis@sheffield.ac.uk (J.L. Provis).

https://doi.org/10.1016/j.cemconres.2019.02.005
Received 31 July 2018; Received in revised form 29 January 2019; Accepted 4 February 2019

Table 1
Approximate temperature profile of an ILW waste package due to GDF emplacement and backfilling [12–15].

Phase of completion		Timescale (years)	Temperature (maximum - °C)
I	Emplacement	50	30–40
II	Care and maintenance	50	30–40
III	Short-term backfill	5	80
IV	Long-term backfill	25	50
V	Post-closure of GDF	–	35–45

Table 2
Major constituents of raw materials, as determined by X-ray fluorescence (XRF) and represented as oxides.

Oxide (wt%)	PC	BFS
CaO	63.7	39.2
SiO_2	20.8	35.1
Al_2O_2	5.1	13.4
Fe_2O_3	2.6	0.2
MgO	2.3	9.9
SO_3[a]	3.7	0.4
Na_2O	0.6	0.2
K_2O	0.8	0.6
TiO_2	0.2	0.8
MnO_2	0.1	0.2
P_2O_5	0.2	–

[a] The SO_3 shown in the BFS oxide composition is most likely present as S^{2-} based on the reducing conditions that prevail during BFS production.

Table 3
Sample reference IDs for the different curing profiles; t is time in days.

Sample name	Curing temperature profile
tA	Samples cured at 35 °C for time, t.
tB	Samples cured at 35 °C for 1 year, then cured at 50 °C for time, t.
tC	Samples cured at 35 °C for 1 year, then cured at 60 °C for time, t.
tD	Samples cured at 35 °C for 1 year, then cured at 80 °C for time, t.
tE	Samples cured at 35 °C for 1 year, then cured at 80 °C for 1 year, and finally cured for 28 days at 50 °C.

[14,15]. In this study heat output of 6 Wm^{-3} was used to model the most extreme scenario (average heat output from low heat generating waste – 1.1 Wm^{-3} until 2040 and declining to 0.5 Wm^{-3} by 2090; heat generation from non-radiogenic mechanisms – 3 Wm^{-3} due to corrosion of waste; microbial degradation of materials – 2 Wm^{-3} [15]).

During the periods of transporting and storing the waste packages within excavated GDF vaults, taking an expected 50 years, the general air temperature was predicted to be 35 °C. A further period of 50 years for care and maintenance is also expected to produce an average air temperature of 35 °C. After the GDF has been filled with waste packages, the vaults will be backfilled with NRVB. The expected heat output from the hydration of the NRVB in an enclosed space, coupled with reduced ventilation within the vault, is expected to raise the temperature of the GDF to a maximum of 80 °C, for a period of 5 years. After this point, the vaults are expected to cool to 50 °C for 25 years, then eventually return to temperatures of 35–45 °C.

Table 5
Elemental correction factors used to correct the SEM-EDS analysis.

Silicon	Aluminium	Calcium	Magnesium	Sulphur
0.97	0.96	0.88	1.00	1.00

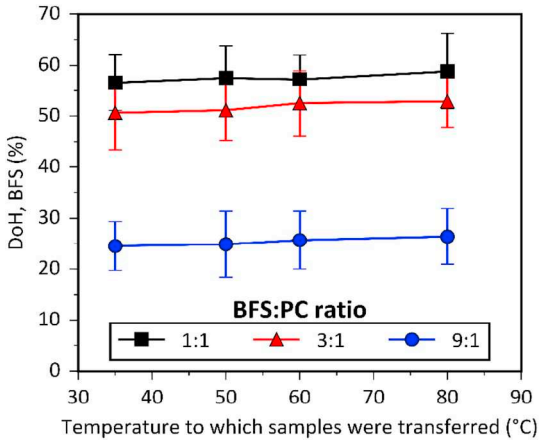

Fig. 1. Degree of hydration (DoH) of BFS determined from EDTA selective dissolution, within BFS-PC blended cements of ratio 1:1, 3:1 and 9:1, for the temperature profiles 360A, 28B, 28C and 28D.

1.2. Effect of temperature on the mineralogy of cements

Changing the temperature of Portland cement alters the mineralogy of the hydrate phases formed [16], including changing the solubility relationships that determine the concentrations of key ions in the pore solution, which define the stability of cement hydrates [17–19].

The solubility relationships that drive formation of calcium silicate hydrate, C-S-H, the dominant binding phase in hydrated PC, are moderately affected by temperature by reducing the solubility products and the concentrations of calcium and silicon required to form C-S-H [17,20]. Martinez-Ramirez and Frías [21], and Bahafid et al. [22], showed that the Ca/Si ratio of C-S-H in hydrated Portland cements decreased with increasing temperature, which resulted in a longer mean chain length (MCL) of the C-S-H, and densification. Similar trends are also observed in Al rich C-S-H (C-A-S-H), forming in Portland cements blended with supplementary cementitious materials (SCMs), presenting an increased silicon content driven by an increased extent of the pozzolanic reaction at higher temperatures [23–25]. At higher temperatures, increased incorporation of aluminium from solution into bridging sites of the C-A-S-H phase also increases the MCL [17,26], as well as the Al/Si ratio [27,28].

Portlandite formation in hydrated PC is only marginally affected by an increase in temperature [16,17,29]. Escalante-Garcia [30,31] showed that during hydration of BFS-PC blends at elevated temperatures, BFS exhibits a greater acceleration in its reaction kinetics than alite. This increasing slag hydration reaction results in increased

Table 4
Comparison of the molar ratios of the BFS, obtained from XRF and SEM-EDS data, and the corrected values obtained by calibration of the EDS data using information from XRF.

	Ca/Si	Si/Ca	Al/Si	Al/Ca	Ca/Al	Mg/Si	Mg/Al	Mg/Ca
XRF	1.20	0.85	0.45	0.38	2.63	0.42	0.94	0.36
Original EDS (μ ± σ)	1.32 ± 0.13	0.76 ± 0.10	0.45 ± 0.05	0.34 ± 0.06	2.90 ± 0.46	0.40 ± 0.04	0.90 ± 0.10	0.31 ± 0.05
Post-corrections	1.20	0.84	0.44	0.38	2.66	0.41	0.93	0.35

consumption of portlandite and leads to a further reduction in portlandite content in the system [23,25].

It has been well documented that ettringite ($Ca_3Al_2O_6{\cdot}3CaSO_4{\cdot}32H_2O$) becomes less stable above 48 °C in hydrated PC and blended cement systems [16,18,19,32]; above 48 °C, AFm-structured calcium monosulphoaluminate ('monosulphate' - $Ca_3Al_2O_6{\cdot}CaSO_4{\cdot}12H_2O$) becomes the dominant sulphoaluminate phase [33,34] up to ~80 °C. Carbonate AFm phases ('monocarbonate' - $Ca_3Al_2O_6{\cdot}CaCO_3{\cdot}11H_2O$ and 'hemicarbonate' - $Ca_3Al_2O_6{\cdot}0.5CaCO_3{\cdot}12H_2O$) are also stable up to 40–90 °C [18].

Silica-free hydrogarnet (katoite - $Ca_3Al_2(OH)_{12}$) is stable at temperatures above 8 °C, however SO_4^{2-} and CO_3^{2-} tend to destabilise katoite in favour of sulphate or carbonate AFm phases up to 55 °C [18,32,35,36]. Siliceous hydrogarnet ($Ca_3Al_2(SiO_4)_y(OH)_{4(3-y)}$; $0 < y < 3$) has been synthesised at temperatures up to 350 °C [37], and at higher temperatures, more $[SiO_4]^{4-}$ ions replace the OH^- ions. At lower temperatures (25–55 °C), the higher pH in hydrated PC drives the solid solution towards a higher OH^- content, thus reducing the silicon uptake in this phase. When the temperature increases, the pH drops and siliceous hydrogarnet is more stable than katoite or AFm phases [35].

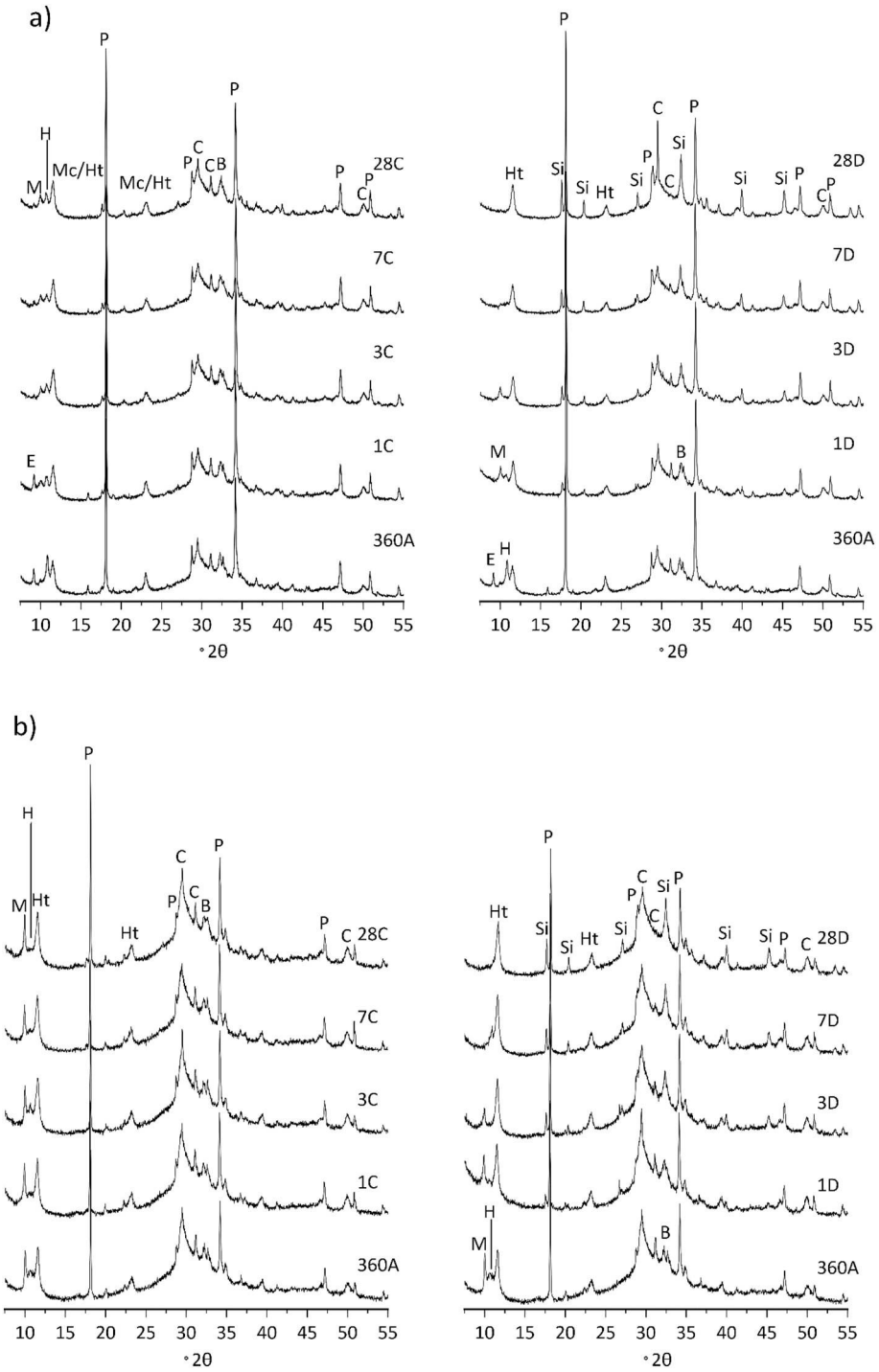

Fig. 2. XRD patterns of a) 1:1, b) 3:1 and c) 9:1 BFS-PC samples cured at 35 °C for 1 year (360A) and then at either 60 °C (tC) or 80 °C (tD) for a further 28 days. Phases identified are: C – C-A-S-H, P – portlandite, E – ettringite, M – monosulphate, H – hemicarbonate, Mc – monocarbonate, Ht – hydrotalcite, B – belite, and Si – siliceous hydrogarnet.

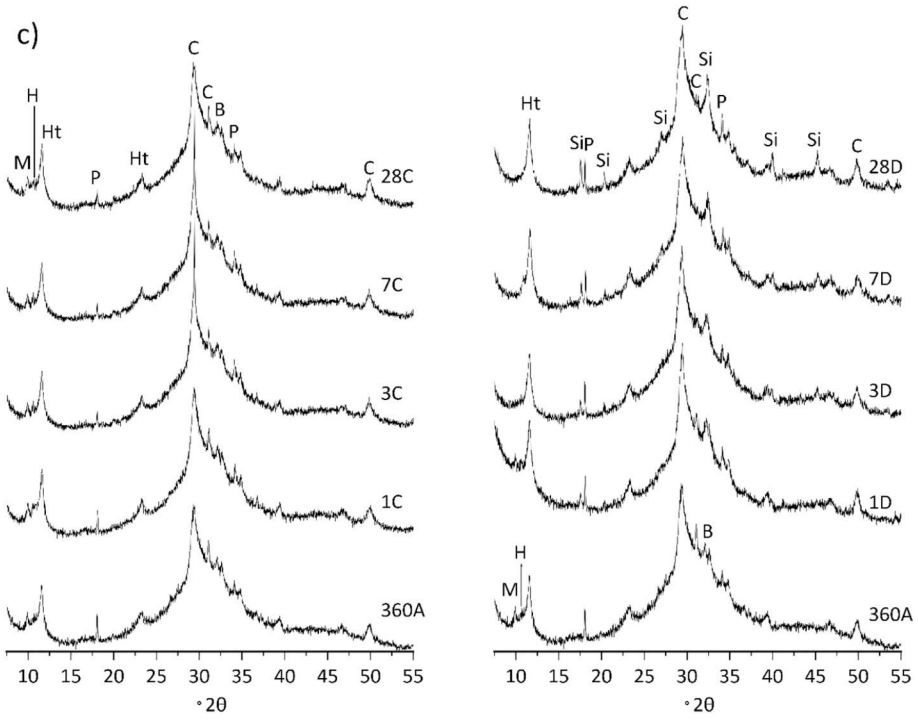

Fig. 2. (*continued*)

Hydrotalcite-group layered double hydroxide (LDH) type phases ($Mg_{(1-x)}Al_x(OH)_{(2+x)}{\cdot}mH_2O$, $0.2 \leq x \leq 0.33$) [38] are prominent in blended or alkali-activated cements due to the high levels of magnesium and aluminium in the precursor materials [39–41]; these remain stable throughout the temperature range of interest here (30–80 °C).

It is essential to understand how temperature changes in the context of a GDF will affect the hydrate phases in blended cements that encapsulate ILW, to enable reliable prediction of how the waste packages will evolve over the millennia that they will be stored. Therefore, this study considers the influence of temperature changes on cured BFS-PC cements with varying BFS:PC ratios and temperature profiles, to simulate anticipated GDF conditions. It should be noted that no interaction with the backfill material or groundwater is described in this work; the scope of this study relates solely to the performance of the wasteforms themselves. Thermodynamic modelling has been shown to accurately and reliably predict the stability of cement hydrate phases under different conditions [16,18,41]. Therefore, thermodynamic modelling can predict phase assemblage, and hence enabling to infer how cementitious wasteforms may perform under GDF conditions.

2. Experimental methodology

2.1. Mix design

Cementitious grouts with ratios of 1:1, 3:1 and 9:1 BFS:PC (compositions in Table 2) were produced with a water/solids (w/s) mass ratio of 0.35, to span the formulation envelope for UK ILW grouts. The precursor materials used were Ribblesdale CEM I 52.5N PC and Port Talbot ground granulated BFS (BS EN 15167-1 GGBS), supplied by the National Nuclear Laboratory. The oxide compositions of the precursors used are displayed in Table 2. Samples were mixed in batches then poured into 50 mL tubes, sealed, and cured in an oven according to the specified temperature regime (see below) until testing.

After 360 days of curing at 35 °C, the samples were transferred to ovens at either 50 °C, 60 °C or 80 °C. Samples were analysed 1, 3, 7 and 28 days after being transferred to the higher temperature ovens, and also 360 days after being transferred to an oven at 80 °C. Additional samples that had been cured at 35 °C for one year and exposed to 80 °C for another year were then transferred to an oven at 50 °C for 28 days. Samples were also cured at 35 °C for up to 720 days as a reference point. The notation used throughout the manuscript for each temperature profile is summarised in Table 3. While the timeframes used in this study do differ from those shown in Table 1 for reasons of practicality, this was deemed the most suitable approach to testing the applicability of thermodynamic modelling to these systems.

2.2. Analytical techniques

Upon reaching the specified testing exposure time, hardened specimens were crushed and ground using acetone as a lubricant, to a particle size below 63 μm. The powders were then submerged in acetone for 15 min and vacuum filtered, to ensure that hydration had ceased [42].

Analysis of mineralogy was performed using powder X-ray diffraction (XRD) on a Bruker D2 Phaser instrument with Cu Kα radiation (1.54 Å) and a nickel filter. Scans were conducted with a step size of 0.020°, for 2 s per step, with front-loading sample holders. The Inorganic Crystal Structure Database (ICSD) and the Powder Diffraction File (PDF) were used in phase identification.

Scanning electron microscopy (SEM) was performed using a Hitachi TM 3030 instrument with a 20 kV accelerating voltage, a working distance of 8 mm and a backscatter detector. Samples were cut and polished using non-aqueous lubricants immediately prior to analysis. An evenly distributed selection of points across a representative 400 μm × 400 μm section of the sample was analysed using a Bruker Quantax 70 X-ray energy dispersive spectroscopy (EDS) detector to determine chemical compositions.

Comparison of the EDS data with the XRF results for the BFS was performed to provide an external calibration for the EDS results on the basis of molar elemental ratios (Table 4). The EDS data analysis was conducting using 20 points from each of 5 identifiable slag grains that were embedded in the grout matrix of the 9:1 system that had been hydrated for 360 days at 35 °C; the points selected were for areas which had clearly not undergone any hydration.

A slight difference between some of the molar ratios was observed when comparing the EDS and XRF results, particularly the ratios

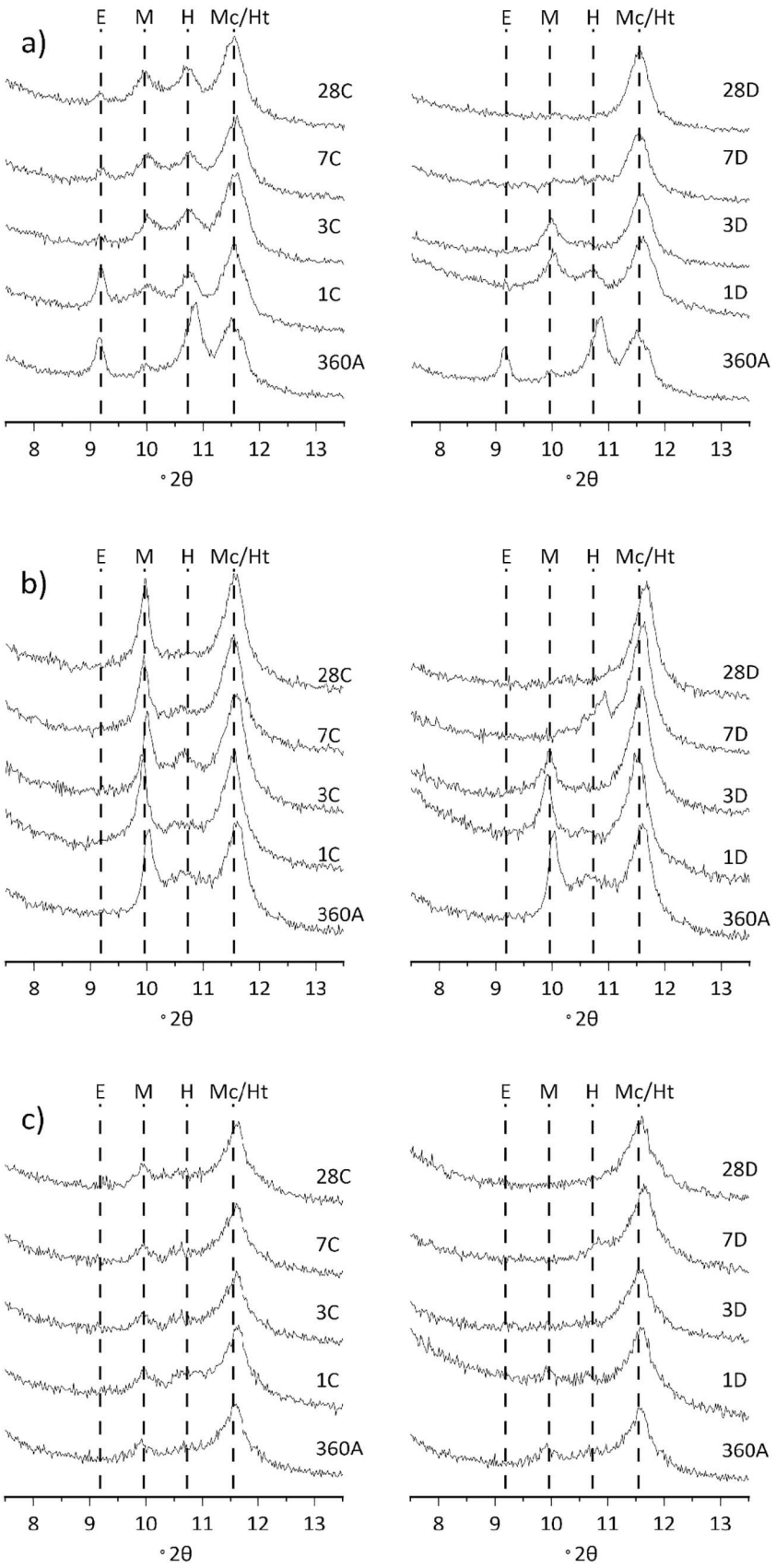

Fig. 3. Highlighted low-angle regions of the XRD patterns of a) 1:1, b) 3:1 and c) 9:1 BFS-PC samples cured at 35 °C for 1 year and then at either 60 °C (C) or 80 °C (D) for up to 28 days. Phases identified are: E – ettringite, M – monosulphate, H – hemicarbonate, Mc – monocarbonate, and Ht – hydrotalcite.

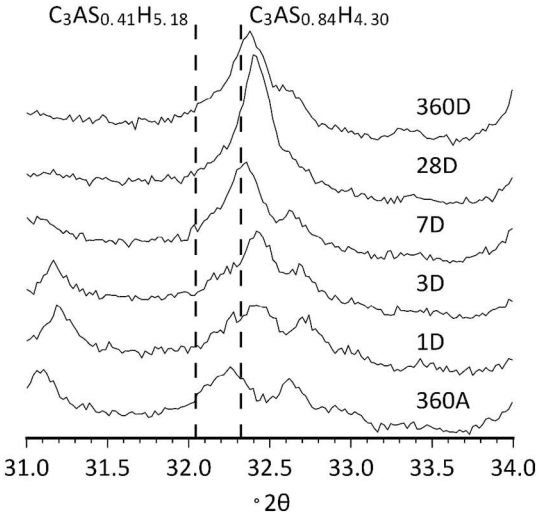

Fig. 4. XRD patterns for 1:1 BFS:PC cements after curing at 35 °C for one year and being transferred to 80 °C for up to 360 days (temperature profile D). The $C_3AS_{0.41}H_{5.18}$ and $C_3AS_{0.84}H_{4.30}$ chemical formulae depict the siliceous hydrogarnet phases available in the CEMDATA14 database.

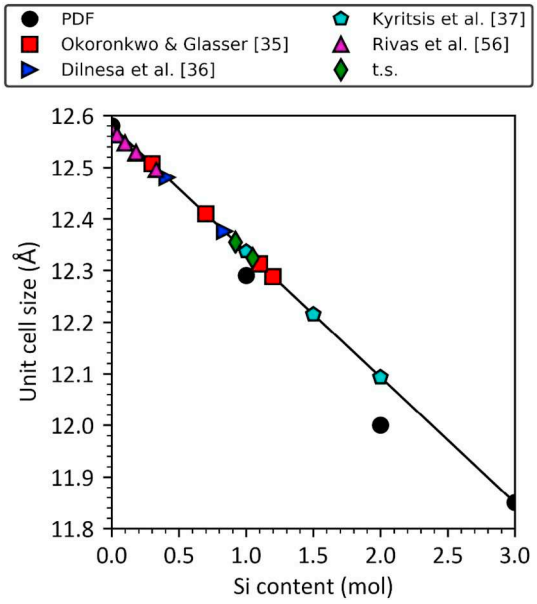

Fig. 5. Unit cell size as a function of Si-hydrogarnet composition: PDF data used include card numbers 24–0217 (a = 12.57 for C_3AH_6); 32–0151 (a = 12.29 for C_3ASH_4); 31–0250 (a = 12.00 for $C_3AS_2H_2$) and 33–0260 (a = 11.846 for C_3AS_3). References include: [35–37,56] and t.s. = this study.

containing calcium and magnesium. As the EDS was conducted on a benchtop SEM instrument, its precision is expected to be challenged by the differences in interaction volume in elemental analysis for lower vs. higher atomic number elements [43], and the difficulty in mapping of oxygen [44,45]. Using a linear regression solver, correction factors for the measured EDS intensities of silicon, aluminium, calcium and magnesium were created to best match the EDS molar ratios to the XRF results, Table 5. These correction factors were applied to calibrate the point analysis data obtained for the hydrated samples.

Degree of hydration values for the Portland clinker and BFS in each blend after 360 days at 35 °C were taken from Prentice et al. [46]. For samples that were cured for longer durations, the degree of hydration of slag was determined using the same selective dissolution technique as described in [46].

Thermodynamic modelling was performed using GEM-Selektor v3 (GEMS) [47,48] using the CEMDATA14 database which is an updated version of CEMDATA07 [16]. Activity coefficients for aqueous species were determined using the Truesdell-Jones extension to the Debye-Hückel equation [49]:

$$\log_{10}\gamma_i = \frac{-A_\gamma z_i^2\sqrt{I}}{1 + \dot{a}B_\gamma\sqrt{I}} + b_\gamma I + \log_{10}\frac{X_{jw}}{X_w} \quad (1)$$

Here, γ_i and z_i are the activity coefficient and charge of the i^{th} aqueous species respectively, A_γ and B_γ are temperature and pressure dependent coefficients, I is the molal ionic strength, X_{jw} is the molar quantity of water, and X_w is the total molar amount of the aqueous phase. A common ion size parameter, $\dot{a}$ (3.67 Å) and short-range interaction parameter, b_γ (0.123 kg/mol), were used, treating KOH as the background electrolyte [49,50].

Mineral phases within CEMDATA14 are recorded at standard conditions (298 K and 1 atm), therefore temperature corrections for the apparent Gibbs energy of formation, $\Delta_a G_{T_0}{}^0$, of these minerals are required to extrapolate to the temperatures of interest, T. Integration of the heat capacity function (Eq. (2)) is used in GEMS [16,19,32]:

$$\Delta_a G^0_T = \Delta_f G^0_{T_0} - S^0_{T_0}(T - T_0) - \int_{T_0}^{T}\frac{C^0_p}{T}dT = \Delta_f G^0_{T_0} - S^0_{T_0}(T - T_0) - a_0\left(T\ln\frac{T}{T_0} - T + T_0\right) - a_1(T - T_0)^2 - a_2\frac{(T - T_0)}{2T\cdot T_0^2} - a_3\frac{(\sqrt{T} - \sqrt{T_0})^2}{\sqrt{T_0}} \quad (2)$$

where $\Delta_f G_{T_0}{}^0$ is the standard Gibbs energy of formation, $S_{T_0}{}^0$ is the standard absolute entropy at T_0 = 298 K, $C_p{}^0$ is the heat capacity, and a_0, a_1, a_2, and a_3 are the empirical coefficients of the heat capacity equation $C_p{}^0 = a_0 + a_1T + a_2T^{-2} + a_3T^{-0.5}$. The apparent Gibbs free energy of formation, $\Delta_a G_{T_0}{}^0$, refers to the free energies of the elements, and $S_{T_0}{}^0$ is the standard absolute entropy at T_0 = 298 K.

Table 6
Molar ratios of common cement phases (precursors and hydrates) which may affect the chemical composition measurements.

Phase	Chemical formula	Al/Ca	Si/Ca	S/Ca	Mg/Al	Al/Si	Ca/Si
Alite	C_3S	–	0.33	–	–	–	3.00
Belite	C_2S	–	0.50	–	–	–	2.00
BFS	–	0.38	0.85	–	0.90	0.45	1.20
Siliceous-Hydrogarnet (Si molar ratio = 1.0)	C_3ASH_4	0.67	0.33	–	–	2.00	3.00
Siliceous-Hydrogarnet Hydrogarnet (Si molar ratio = 0.84)	$C_3AS_{0.84}H_{4.3}$	0.67	0.28	–	–	2.38	3.57
Katoite	C_3AH_6	0.67	0.00	–	–	–	–
C-A-S-H (Ca/Si = 1.2, Al/Si = 0.1)	$C_{1.2}A_{0.1}SH$	0.17	0.83	–	–	0.20	1.20
C-A-S-H (Ca/Si = 1.4, Al/Si = 0.075)	$C_{1.4}$ $A_{0.075}SH$	0.11	0.71	–	–	0.15	1.40
C-A-S-H (Ca/Si = 1.6, Al/Si = 0.05)	$C_{1.6}A_{0.05}SH$	0.06	0.63	–	–	0.10	1.60
Ettringite (AFt)	$C_6A\underline{S}_3H_{32}$	0.33	–	0.50	–	–	–
Monosulphate (AFm)	$C_4A\underline{S}H_{12}$	0.50	–	0.25	–	–	–

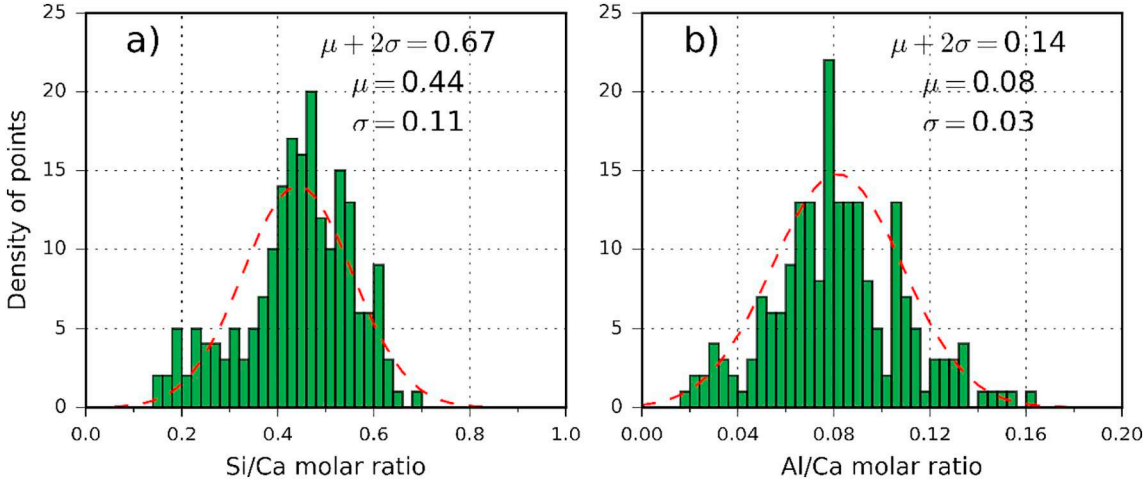

Fig. 6. Histograms of the molar ratios of spot analyses of the 1:1 BFS-PC cement cured at 35 °C for 360 days, showing a) Si/Ca and b) Al/Ca molar ratios determined from calibrated SEM-EDS analysis.

3. Experimental results and discussion

3.1. Degree of hydration of BFS

In all blends, BFS hydration increased slightly when transferring a sample that had been cured at 35 °C for a year to a higher curing temperature for an additional 28 days (Fig. 1), consistent with previously reported data showing that BFS hydration in BFS-PC cements increases at higher temperature [31,51]. However, the maximum increase in hydration degree was 2.2%, as the majority of the anhydrous material had already reacted during the first year of curing at 35 °C, and variations of the calculated values lie within the experimental errors. A lack of pore space due to the initially low w/s used for producing the assessed cements (w/s 0.35) may also have restricted the further hydration after one year of curing. For curing regimes 360D and 28E, each blend showed an increase of no > 2% in BFS hydration degree beyond the degree reached for a given condition (i.e. the 80 °C point in Fig. 1).

3.2. X-ray diffraction and qualitative analysis

3.2.1. Effect of curing temperatures at 60 and 80 °C

The powder diffraction patterns for the cement pastes cured with temperature profiles 1 to 28C and 1 to 28D (i.e. pastes transferred to 60 or 80 °C after a year at 35 °C), with 360A as a reference point, are presented in Fig. 2. All pastes show some residual belite peaks; there are also minor contributions from alite and ferrite clinker components (see Section 4.1), although these are too small to mark on Fig. 2.

The three formulations showed minimal loss or alteration of portlandite (ICSD #15471), or C-A-S-H formation, when exposed to higher temperatures for 28 days after initial curing at 35 °C for one year. In the 3:1 and 9:1 cements after 1 and 3 days at both 60 and 80 °C, the peak at 29.4° 2θ attributed to a C-A-S-H type phase resembling Al-substituted tobermorite (PDF #34-0002) becomes sharper as the sudden elevation in temperature causes a spike in crystallinity of the C-A-S-H phase. After 28 days of curing at high temperature the reflection broaden and the sharpness become less prominent, which is attributed to lengthening of the aluminosilicate chains with silicate polymerisation at elevated temperature [52,53], inducing some structural disorder.

The impact of temperature on the sulphate and carbonate AFm and AFt type phases can be observed in Fig. 3. Ettringite (ICSD #16045) was only observed in the 1:1 cement after 360 days at 35 °C. After 3 days at 60 °C, the majority of the ettringite reflection peak was depleted, indicating that ettringite had been destabilised at higher temperature. This depletion was completed within 1 day at 80 °C. At both of these temperatures, the resulting release of sulphate into the pore solution led to the formation of monosulphate (ICSD #100138).

The monosulphate peak intensity increased continuously with time in the samples transferred to 60 °C because of the decomposition of ettringite; this also occurs in the 80 °C samples up until 3 days. However, after 7 days at 80 °C, monosulphate can no longer be observed in the 1:1, 3:1 or 9:1 cements, although it persists at a curing temperature of 60 °C in the 1:1, 3:1 and 9:1 cements after 28 days.

Depletion of the hemicarbonate (PDF #00-036-0129) reflection intensity at 60 °C was observed in the 1:1 and 3:1 systems after 28 days at elevated temperature. This is attributed to depletion of OH^- ions corresponding to the known phenomenon of a pH drop at increased temperature [19]. There is some overlap of the main reflection peaks assigned to monocarbonate (approx. 11.7° 2θ, PDF #00-036-0377) and the broader peak attributed to the hydrotalcite-like LDH (11.2–11.6° 2θ, PDF #00-014-0525), making it difficult to differentiate between these two phases [54]. Similarly to the sulphate-containing AFm phases, after 28 days at 80 °C, hemicarbonate peaks were no longer observable, and the remaining peak at 11.6° 2θ was most likely to represent hydrotalcite-like LDH. The significantly lower solubility of magnesium and aluminium [55] from the hydrotalcite-like LDH caused this phase to persist at higher temperatures. The peak at 11.6° 2θ may be attributed to monocarbonate, however due to the low content of carbonate in the system, this phase was unlikely to persist at this temperature.

In general, hydrates containing higher contents of water became destabilised by the increase of temperature more rapidly than those with lower water content. This is evident through the persistence of the portlandite (2 mol of water per formula unit), C-A-S-H phase (2–4 mol of water), and the formation of siliceous hydrogarnet (3–6 mol of water) at 80 °C. The exception to this trend was hydrotalcite-like LDH (10–14 mol of water), as this phase is more stable against dissolution as mentioned above, and there are not obvious less-hydrated magnesium aluminates to which it could be converted in this temperature range.

3.2.2. Siliceous hydrogarnet ($Ca_3Al_2(SiO_4)_{3-y}(OH)_{4y}$) formation at 80 °C

Within the CEMDATA14 database used in GEMS, there are two forms of siliceous hydrogarnet: $C_3AS_{0.41}H_{5.18}$ and $C_3AS_{0.84}H_{4.30}$. Understanding which phase to use in this instance was based upon the method of Dilnesa et al. [36], and Okoronkwo and Glasser [35]. The silicon content of the cubic siliceous hydrogarnet structure was determined using the lattice parameter *a*, obtained from XRD analysis and interpolating between grossular (C_3AS_3) and katoite (C_3AH_6) on a linear scale; Kyritsis et al. [37] and Rivas et al. [56] have shown experimentally that this method is effective, and highlighted the miscibility gap between $C_3AS_{0.41}H_{5.18}$ and $C_3AS_{0.84}H_{4.30}$. The lattice parameter values for $C_3AS_{0.41}H_{5.18}$ and $C_3AS_{0.84}H_{4.30}$ are 12.480 and

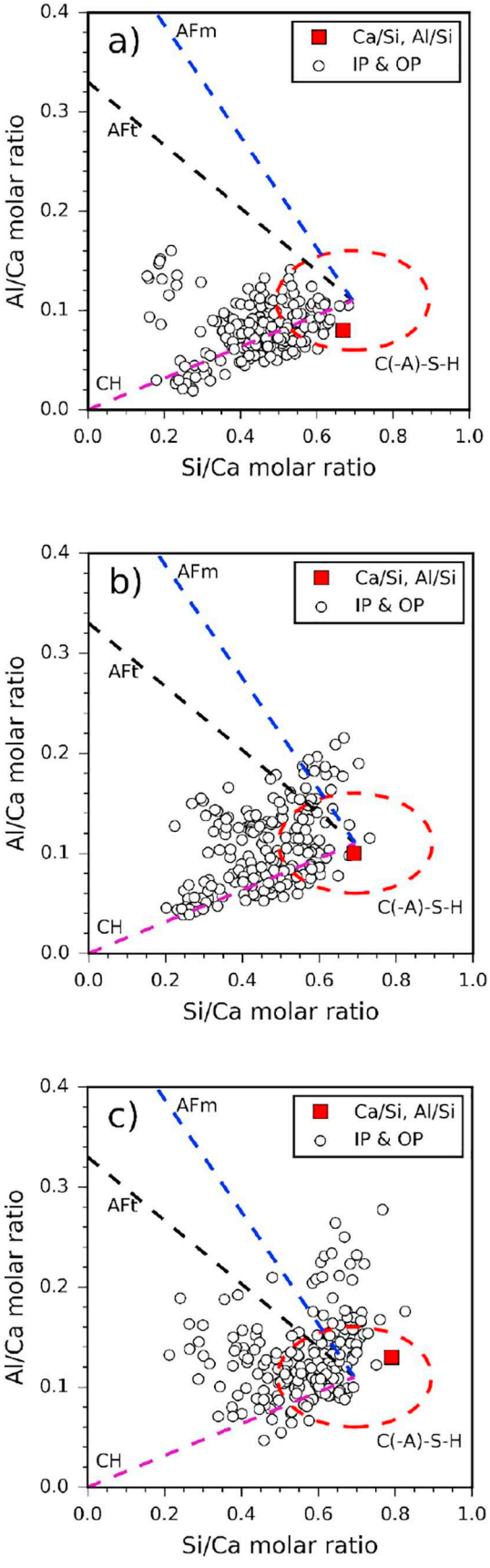

Fig. 7. Al/Ca versus Si/Ca graph of the a) 1:1 b) 3:1 and c) 9:1 BFS-PC cement cured at 35 °C for 360 days. The dashed oval highlights the region where a C-A-S-H phase with Ca/Si ~1.0–1.6 and Al/Si ~0.1–0.2 would appear. The tie lines leading from the centre of the circle lead to the other prominent cement hydrates which may intermix with C-A-S-H (AFt – ettringite, AFm – monosulphate, CH – portlandite). The red square denotes the statistically determined Ca/Si and Al/Si ratio for the individual formulations. (For interpretation of the references to color in this figure legend, the reader is referred to the web version of this article.)

12.376 Å, respectively, and these were used to determine which form of siliceous hydrogarnet was most similar to the phase formed at 80 °C in the cements used in this study.

From Fig. 4 it is evident that the higher-Si siliceous hydrogarnet phase ($C_3AS_{0.84}H_{4.30}$) was more representative of the phase observed in the XRD data obtained for the BFS-PC cements assessed in this study. The lattice parameter *a* of siliceous hydrogarnet determined using the samples cured at 35 °C for 360 days then at 80 °C for a further 360 days (360D) was 12.355 Å for the 1:1 blend, and 12.324 Å for the 3:1 and 9:1 blends as displayed in Fig. 5. These values equated to a silicon content of 0.92 mol in the 1:1, and 1.05 mol in the 3:1 and 9:1 cements, Fig. 5. The bulk Ca/Si ratio in the 1:1 cement was higher than in the 3:1 and 9:1 cements due to the lower slag replacement, which gave a lower level of silicon replacement within the siliceous hydrogarnet structure. Therefore, when utilising GEMS for the higher temperatures, the higher silicon content solid solution model ($C_3(A,F)S_{0.84}H_{4.30}$) which contained the $C_3AS_{0.84}H_{4.30}$ phase, was used to represent siliceous hydrogarnet, as this was the model within the database that gave the closest correspondence to the experimental results. The additional silicon content observed in the BFS-PC cements evaluated can be attributed to the high availability of silicon and the moderate pH of these cements, which favours incorporation of silicate over hydroxide in the hydrogarnet structure.

3.3. Determination of chemical composition of the C(-A)-S-H phase by SEM

The composition of the C-A-S-H phase was determined by SEM-EDS point analysis, which was conducted manually by choosing 200 points focusing on C-A-S-H regions by selecting points on the darker rims around anhydrous grains and the light grey areas found in the cement matrix. Due to the nature of cement hydration, these areas are intermixed with other hydrate phases. Elemental ratio plots were used similarly to previous studies [24,44,45,57] to determine the least intermixed regions containing C-A-S-H phases, and quantification of the elemental ratios was calibrated as described in Section 2.2 using the XRF and EDS data for anhydrous BFS grains. In a plot of Al/Ca vs. Si/Ca, the high Si/Ca (0.6–1.0) cluster of points represents the composition of the C-A-S-H phase, is summarised by the molar ratio comparisons in Table 6. Durdzinski et al. [45] and Rossen et al. [44] used a statistical approach to determine the area of least intermixing. A point two standard deviations above the mean ($\mu + 2\sigma$) of the distribution of Si/Ca values was deemed to best represent the point of least intermixing; this is larger than 95% of values assuming a normal distribution, and is therefore considered one of the highest Si/Ca values which can best describe pure C-A-S-H phases. The mean Al/Ca value is used to define the molar content of aluminium within C-A-S-H phases [44,45]. Dividing the Al/Ca by the Si/Ca value, it was possible to obtain the Al/Si value of the C-A-S-H phases.

An example of the analysis of the 1:1, 3:1 and 9:1 BFS:PC formulations after 360 days of curing at 35 °C can be seen in Fig. 6 and Fig. 7. The histogram plots shown in Fig. 6 show the Si/Ca and Al/Ca values obtained from the EDS measurement of the 1:1 BFS-PC blend, which appear to be well described by a normal distribution. Most of the data points fall outside of the C-A-S-H phase region, shown in Fig. 7; this is expected for these blended cement systems because of the intimate intermixing of hydrate species on a length scale finer than the

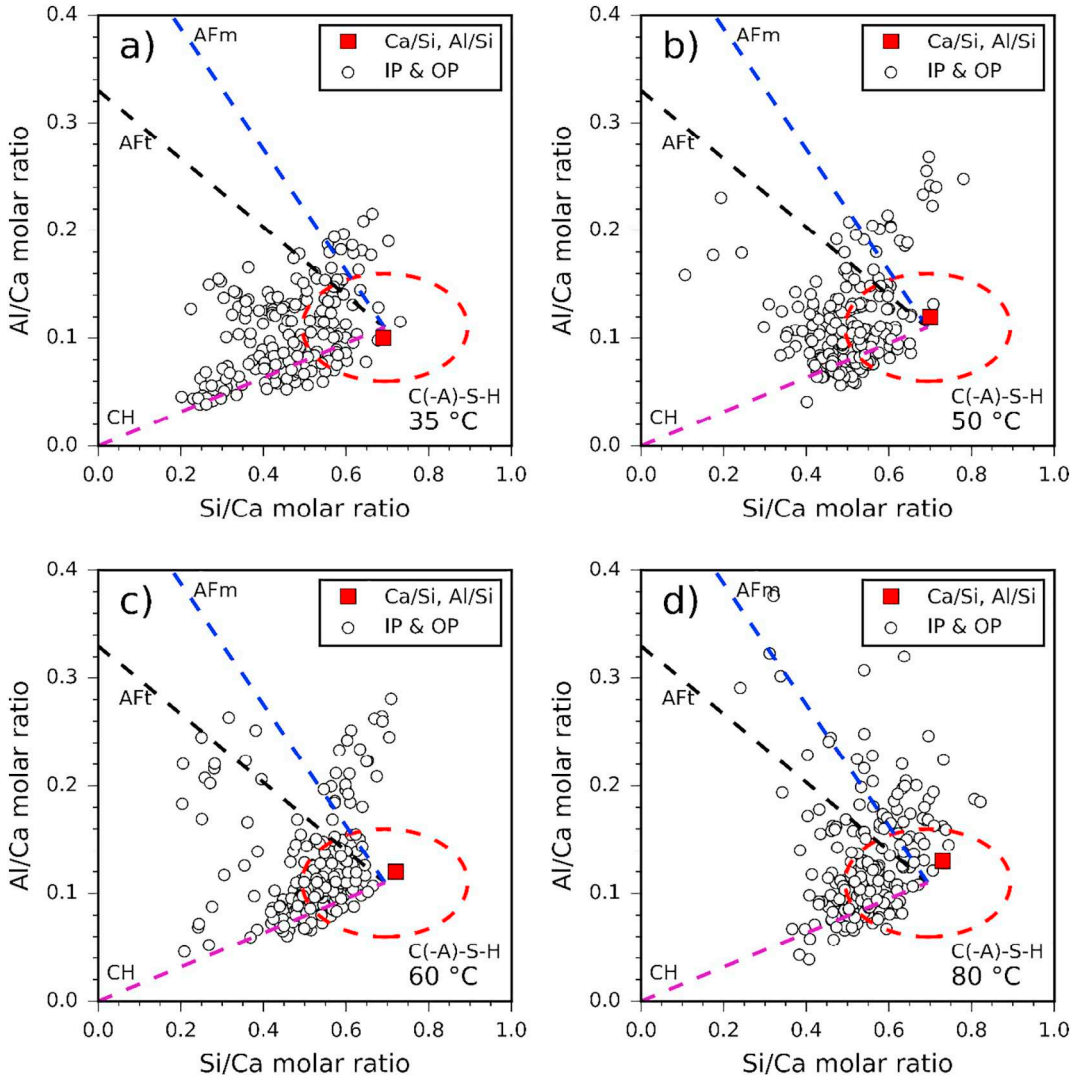

Fig. 8. Al/Ca versus Si/Ca graphs for the 3:1 BFS-PC cement cured at 35 °C for 360 days and then exposed to (a) 35 °C, (b) 50 °C, (c) 60 °C and (d) 80 °C for a further 28 days. The dashed oval highlights the region where a C-A-S-H phase with Ca/Si 1.0–1.6 and Al/Si 0.1–0.2 would appear. The tie lines leading from the centre of the circle lead to the other prominent cement hydrates which may intermix with C-A-S-H (AFt – ettringite, AFm – monosulphate, and CH – portlandite). The red square denotes the statistically determined Ca/Si and Al/Si ratio for the individual formulations. (For interpretation of the references to color in this figure legend, the reader is referred to the web version of this article.)

EDS analysis spot size. However, there is clear evidence that the monosulphate and ettringite phases are heavily intermixed and varied within the sample, since not many of the points follow a distinct tie line to the other phases. Ettringite, monosulphate, hemicarbonate and monocarbonate may all shift the spread of data points to higher Al/Ca values, as summarised in Table 6.

This approach can also be applied to the 80 °C samples, although the siliceous hydrogarnet also contains silicon and will consequently influence the Si/Ca values observed. The maximum Si/Ca value the siliceous hydrogarnet may exhibit, based on the lattice parameter data, is 0.35. Fig. 8 highlights the impact of siliceous hydrogarnet on the 3:1 cement at 35, 50, 60 and 80 °C. There was clear evidence of siliceous hydrogarnet EDS data points at 80 °C.

The backscattered electron (BSE) images in Fig. 9a–d highlight the variation of the morphology of the 3:1 BFS-PC cement cured at different temperatures. Region 1 in Fig. 9a represents a fully hydrated BFS particle and the inner-product C-A-S-H phase (intermixed with hydrotalcite-group LDH) in close proximity to the slag grain. Region 2 in Fig. 9b highlights the more porous structure of the outer-product C-A-S-H phase which forms within the initially fluid-filled space of the cement matrix. These regions appeared denser at higher temperatures, specifically highlighted in the 80 °C sample in region 3. Region 3 appears from its angular shape to have been a slag grain similar to region 1, but which has almost fully dissolved. Other hydrated and partially hydrated slag grains are observed in regions 4 and 5, respectively.

A decrease in Ca/Si and increase of Al/Si ratio (Table 6 in [58]) at higher temperature was observed across the three formulations. Condensation reactions of the monomeric and dimeric silicates may lead to an expulsion of calcium ions and water from the C-A-S-H phase, leading to higher polymerisation of the gel at increasing temperatures [53], consistent with this observation. The Ca/Si decrease was greatest in the 1:1 BFS-PC blend, with the ratio decreasing by as much as 0.1 units from 35 °C to 80 °C. The Ca/Si decrease may be more prominent in the 1:1 formulation because there was more available Ca to be redistributed upon a change in temperature. This may be the cause of the greater variation in the Ca/Si observed in the work of Bahafid et al. [22] compared with the work of Burciaga-Diaz et al. [59]: Bahafid et al. considered a high Ca/Si class G cement and observed a drop in Ca/Si by 0.2 between 25 and 90 °C, whereas Burciaga-Diaz et al. studied alkali-activated slag cement systems (with much less Ca than class G cement) at 20 and 60 °C in which there was no clear overall change in the Ca/Si or Al/Si values.

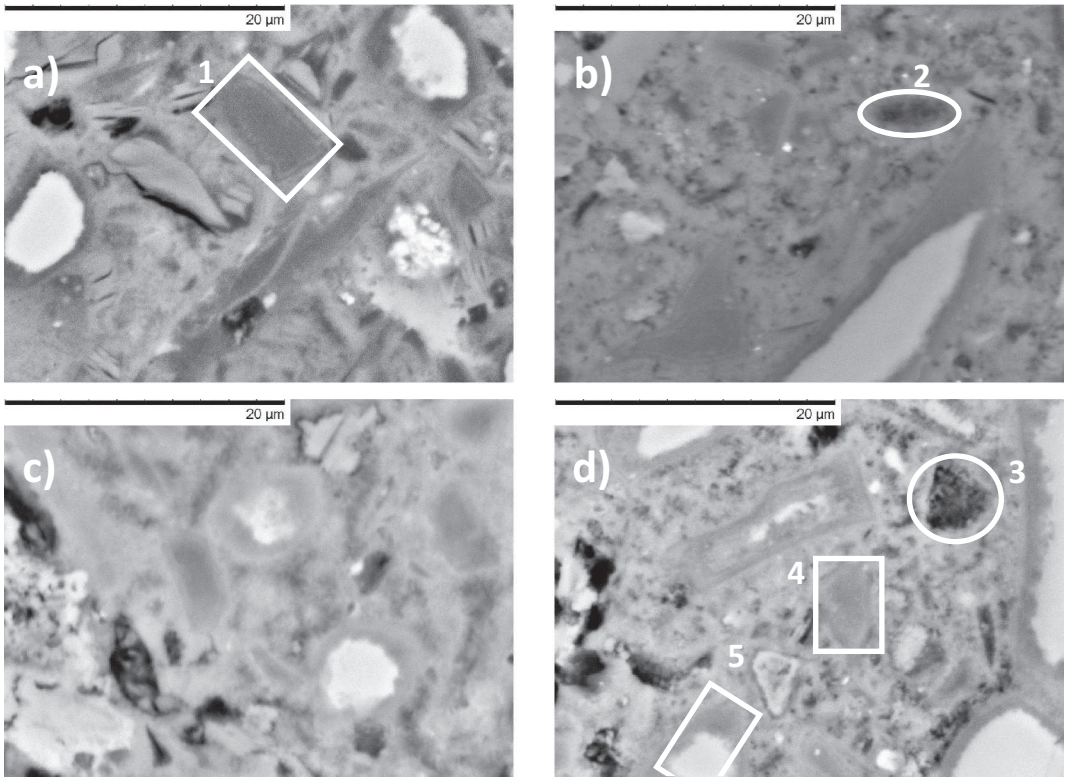

Fig. 9. BSE-SEM images of 3:1 BFS-PC cement cured at a) 35 °C for 360 days and then exposed to b) 50 °C, c) 60 °C, and d) 80 °C for a further 28 days.

Table 7
Clinker degree of hydration values used in thermodynamic modelling. Taylor-Bogue analysis determined the clinker phase ratios in the initial PC: C_3S = 71.9 wt%, C_2S = 6.8 wt%, C_3A = 8.0 wt%, C_4AF = 7.7 wt% [46].

Clinker phase	DoH (%)		
	1:1	3:1	9:1
C_3S	87	93	95
C_2S	68	55	47
C_3A	100	100	100
C_4AF	81	81	81

An increasing abundance of silicate chain sites becoming available as a result of the condensation of calcium silicate species provided an opportunity for aqueous aluminium species to bridge gaps in the silicate chain. The additional opportunity for bridging in the aluminosilicate chains may be the cause for the increase of the Al/Si in all three formulations. The 1:1 formulation displayed the greatest rise in Al/Si ratio, increasing by 0.04 units. The 9:1 formulation exhibited the largest Al/Si values, at Al/Si reaching 0.19.

4. Evaluation of the efficacy of thermodynamic modelling

4.1. Selection of potential phase assemblage constituents

Two modelling approaches were followed in this study, with calculations conducted with ("*SH approach*") and without ("*NS approach*") the presence of a siliceous hydrogarnet; the phases available for hydration are summarised in Table 7 of the accompanying Data in Brief article [58]. A similar methodology was applied by Deschner et al. [24] and by Dilnesa et al. [60] for low pH cements and 3 year old cements, respectively. This approach was intended to ensure the correct phases form at the different temperatures, incorporating restrictions which may be kinetic rather than thermodynamic in foundation. Taylor and Richardson [61] showed that siliceous hydrogarnet does not form in blended cements up to 20 years of curing at 20 °C, therefore highlighting that its inclusion in potential phase assemblages at lower temperatures is unwarranted. Deschner et al. [24] used the SH approach for temperatures above 50 °C, which causes the monosulphate, monocarbonate and hemicarbonate phases to become destabilised as siliceous hydrogarnet is a more stable alternative. In the current study, monosulphate, monocarbonate and hemicarbonate phases were observed up to 60 °C by XRD, and therefore the upper limit of the NS method and the lower limit of the SH method were changed to 60 °C.

Alkali distribution ratios (R_d) to simulate alkali uptake in the C-A-S-H phase were used for sodium and potassium. The distribution ratios calculate the uptake of alkalis from solution based on the mass of C-A-S-H formed and the concentration of alkalis in solution:

$$R_d = \frac{c_s w}{c_d s} \quad (3)$$

where, c_s is the concentration of the alkali in the solid phase (mol/ml), c_d is the concentration of the alkali in solution (mol/ml) and w/s is the water to solid ratio (ml/g). Alkali distribution ratios for Na_2O and K_2O of 2 and 1.2, respectively, were used for C-A-S-H phase for both modelling approaches, following the method of Lothenbach et al. [16]. These values were chosen as they are similar to the values determined by Hong and Glasser [62,63] for C-S-H and C-A-S-H phases with Ca/Si values between 1.2 and 1.6.

A constant degree of reaction of the BFS and clinker phases was used for each system. The DoH of BFS at 60 °C was used for the *NS method* and the DoH of BFS at 80 °C was used for the *SH method* (Fig. 1). The reaction of slag was assumed to be congruent. The DoH values of clinker phases were taken from Prentice et al. [46], with an additional 5% reaction included to replicate the increase of temperature on the clinker phases. A summary of the DoH values can be seen in Table 7. Calcite and gypsum were observed in the anhydrous PC XRD diffractograms, and were quantified by Rietveld analysis (data not shown) to be 4.5 and 3.5 wt%, respectively of the PC fraction of the systems.

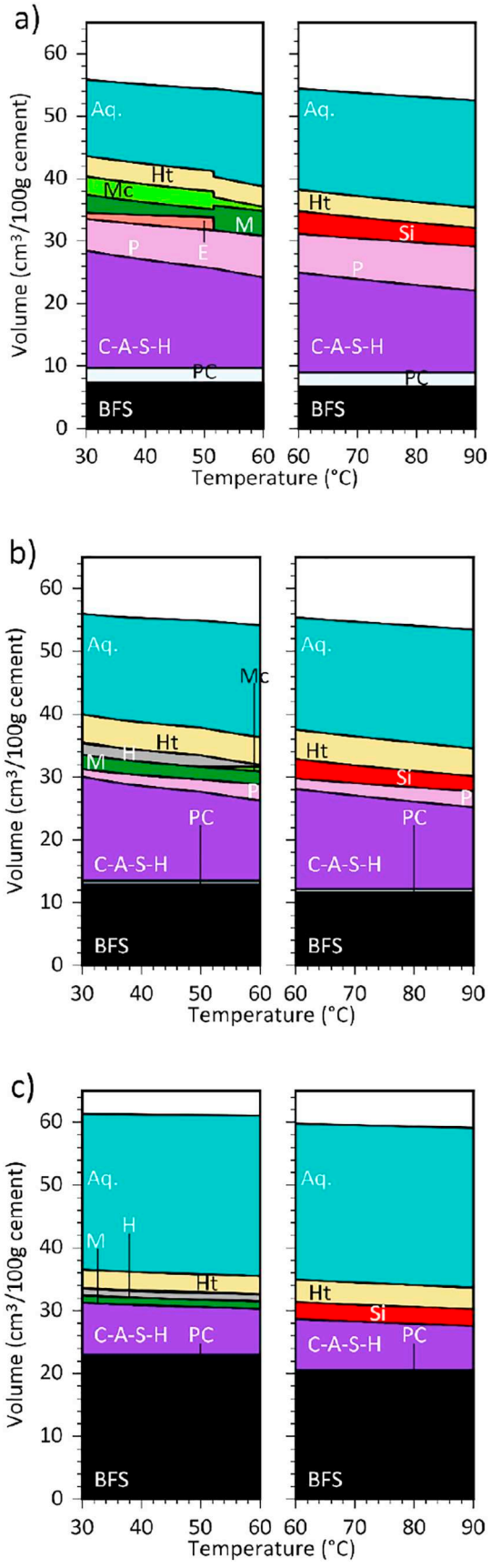

Fig. 10. Phase assemblages of a) 1:1, b) 3:1 and c) 9:1 BFS-PC cements determined using the thermodynamic modelling software GEMS [47]. The prediction of phase formation was determined as a function of temperature while the remnant precursor content was kept constant. Siliceous hydrogarnet was only allowed to form above 60 °C, and each graphic shows a break at this point to reflect the change in model assumptions. The phase notations correspond to: BFS – Blast furnace slag, PC – Portland cement, C – C-A-S-H, P – portlandite, E – ettringite, M – monosulphate, H – hemicarbonate, Mc – monocarbonate, Ht – hydrotalcite, and Si – siliceous hydrogarnet.

4.2. Phase assemblage as a function of temperature

The phases predicted by thermodynamic modelling to form in the 1:1 BFS:PC system exposed to temperatures below 60 °C were C-A-S-H, portlandite, ettringite, monosulphate, monocarbonate and hydrotalcite-like LDH (Fig. 10a). The ettringite phase was no longer stable above 52 °C, consistent with the XRD results of this study where ettringite was still observed up to 50 °C as seen in Fig. 11a and Fig. 3a, and only after 28 days at 60 °C does it appear to have mostly converted into monosulphate. Contrary to the XRD results the ettringite content increases in the thermodynamic modelling up until the point of destabilisation (52 °C). The influence of the C-A-S-H model to withdraw aluminium from solution caused an increased SO_3/Al_2O_3 ratio within the aqueous solution. At the point of 52 °C, sum of the chemical potentials of the aqueous species become more negative than the chemical potential of ettringite and the ΔG becomes positive ($\Delta G_{r,T} = \mu_{ettringite,\ T} - (6\ \mu_{Ca,T} + 2\ \mu_{AlO2-,T} + 4\ \mu_{OH-,T} + 3\ \mu_{SO4-2,T} + 30\ \mu_{H2O,T})$) which causes monosulphate to become the only sulphate phase because monosulphate requires lower Ca^{2+}, AlO_2^-, SO_4^{2-}, OH^- and H_2O concentrations to form, despite the excessive SO_3/Al_2O_3 ratio necessary to form ettringite. Monosulphate, required lower concentrations of the aqueous species formed in place of ettringite. Increasing temperature, increased the SO_4^{2-} concentration in the *NS method*, due to this destabilisation of ettringite as was similar to the Deschner et al. study [24] which considered FA-PC hydration at different temperatures. Within the *SH method*, no sulphate or carbonate containing phases form due to the greater stability of the Ca-Al-Si-OH phases. This resulted in a greater concentration of sulphate in the simulated pore solution of the *SH method* compared to the *NS method*, because all available sulphur in the systems were present in the pore solution in the *SH method*.

The increased sulphate concentration in solution in both methods may have led to increased sulphate adsorption to the C-A-S-H phase [64], however, a sulphate uptake model similar to alkali uptake (Eq. (3)) was not employed in this work and therefore this was not taken into account in the mass balance calculations.

In the experimental results, hemicarbonate was observed at 50 and 60 °C (Fig. 11), however due to the high CO_2/Al_2O_3 ratio in the pore solution, monocarbonate was calculated to be more beneficial to the mass balance in the 1:1 BFS:PC system. Matschei et al. [65] highlighted the importance of the SO_3/Al_2O_3 and CO_2/Al_2O_3 ratios within Portland cement systems, determining which of the sulphate and carbonate AFm or AFt phases form in each specific instance, as there are small energetic differences between various members of these families. In the 1:1 cement the SO_3/Al_2O_3 and CO_2/Al_2O_3 ratios were 0.4 and 0.2, respectively. According to Matschei et al. [65], this pair of ratios should form monosulphate and hemicarbonate. However, due to the presence of the more thermodynamically stable C-A-S-H and hydrotalcite-like LDH phases, which withdraw the aluminium from solution, the effective sulphate and carbonate contents become much higher with respect to Al_2O_3. This causes the thermodynamic model to predict the formation of higher SO_3 and CO_2 rich-phases. Within the 3:1 (Fig. 10b) and 9:1 (Fig. 10c) cements, monosulphate was consistently observed in the modelling and experimental results up to 60 °C. Hemicarbonate became destabilised at higher temperatures in the 3:1 cement, however as CO_2/Al_2O_3 increases with increasing temperature, formation of monocarbonate occurred. The CO_2/Al_2O_3 ratio was consistently lower in the

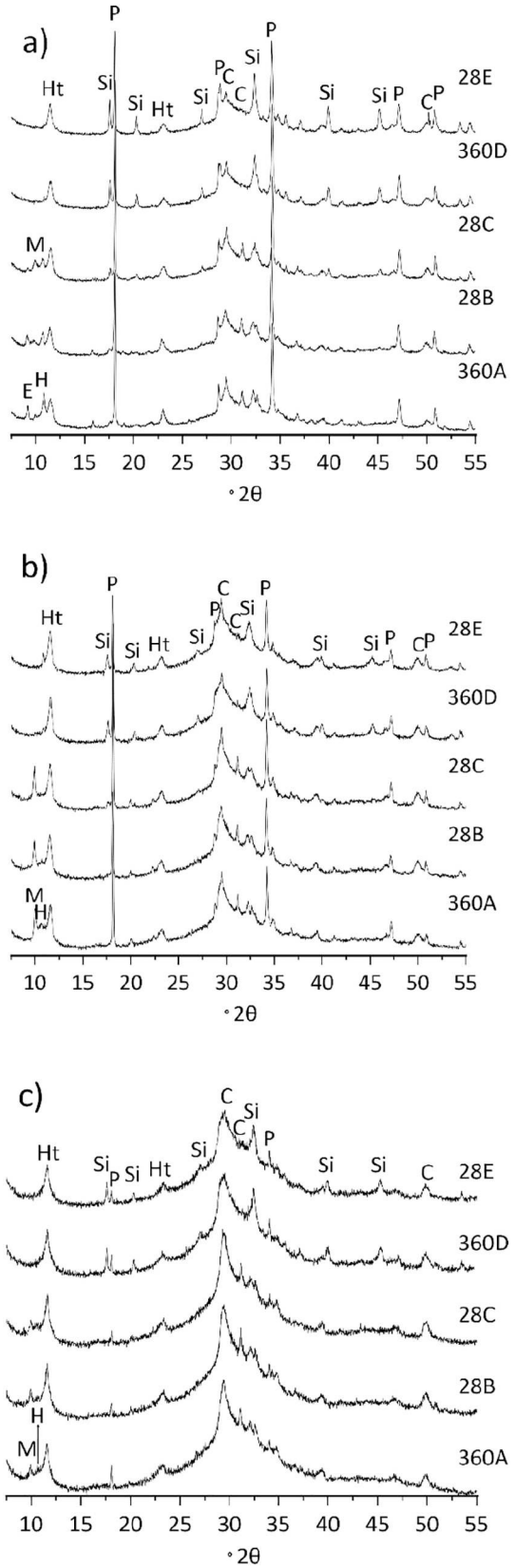

Fig. 11. XRD patterns of a) 1:1, b) 3:1 and c) 9:1 BFS-PC cements exposed to different temperature regimes. Samples cured at 35 °C for 1 year (360A) and then at either 50 °C (tB), 60 °C (tC), 80 °C (tD) for time, t (days), or at 80 °C for 1 year and then at 50 °C for a further 28 days (tE). Phases identified are: C – C-A-S-H, P – portlandite, E – ettringite, M – monosulphate, H – hemicarbonate, Mc – monocarbonate, Ht – hydrotalcite, B – belite and Si – siliceous hydrogarnet.

9:1 cement as this contained the lowest amount of calcite (supplied by the PC), therefore it was possible for hemicarbonate to persist.

A trend of decreasing volume of C-A-S-H and increasing portlandite was observed in the 1:1 and 3:1 blends as the temperature increased. The densification of the C-A-S-H phase at higher Al/Si and lower Ca/Si ratios (see the specific volumes of each end-member in the C-A-S-H model in Table 7 in the accompanying Data in Brief paper [58]) led to a decreasing volume of the C-A-S-H phase as temperature increased. More calcium is available for formation of other phases as a result of the decreasing Ca/Si of the C-A-S-H, therefore the volume of portlandite increases.

Thermodynamic modelling appropriately describes the phases forming at the various temperatures investigated, however simulating the decrease of temperature from 80 °C to 50 °C using the *NS* and *SH* methodology may not be as effective. Fig. 11 shows that the phases observed experimentally were the same as those predicted using the *SH method*, however the suggested protocol of determining the phase assemblage up to 60 °C disagrees with the recorded phase assemblage for the tE temperature profile, where the sample has been held at 80 °C for an extended period before returning to lower temperature. Therefore, it is recommended that once the cement has reached a temperature at which the siliceous-hydrogarnet phase may form, the *SH method* must be used to accommodate this change. This gives further indication that the limitation on formation of siliceous hydrogarnet at near-ambient temperature is kinetic rather than thermodynamic, as this phase persists after cooling once it has formed at higher temperature. Conversely, it is possible that a longer period at 50 °C may be necessary to determine whether the phase assemblage will re-equilibrate to a hydrogarnet-free state in the very long term.

The possibility that the waste packages may reach a temperature of 80 °C is still considered the most extreme scenario for use in safety case development, providing an upper limit on what may occur in practice [12].

Volume expansion of the hydrates is not expected based on the results from Fig. 10. If it did take place, this would be a cause of concern for potential cracking in the waste packages. The reduced possibilty of cracking can be seen as a positive to reinforce the notion that cement encapsulation is a viable option for long-term storage of ILW. Small levels of shrinkage are expected as a result of the densification of the C-A-S-H phase.

4.3. Chemical composition of C-A-S-H phase using thermodynamic modelling as a function of temperature

The different phases allowed to form within a simulation of hydration of cements affect the predicted composition of the C-A-S-H phase (Fig. 12). The *NS method* predicted a decline in Ca/Si and an increase in Al/Si for each cement up to 60 °C, coinciding with what was determined from SEM-EDS analysis. A notable decrease in the Ca/Si ratio (Fig. 12a), with an increase in Al/Si (Fig. 12b), was observed at 52 °C and 50 °C in the 1:1 and 3:1 cements, respectively, in the thermodynamic model outputs. This is caused by the decomposition of ettringite in the 1:1 BFS:PC system and the conversion of hemicarbonate to monocarbonate in the 3:1 cement. In each case, it is likely that an increase in aluminium concentration in the pore solution caused the sharp rise of Al/Si within the C-A-S-H phase.

As a result of the dominance of the hydrogarnet phase in the *SH method*, a more consistent pattern in Ca/Si and Al/Si values was observed in those simulations. The highly stable siliceous hydrogarnet competes with the C-A-S-H phase for the calcium, aluminium and silicon in the system. Dilnesa et al. [36] highlighted the minimal effect of increasing temperature on the $C_3AS_{0.84}H_{4.3}$ hydrogarnet phase. Accordingly, the Ca/Si value of the 9:1 system described by the *SH model* did not vary a great deal (Fig. 12a) because of the strong competition for the available silicon and calcium between the two phases: C-A-S-H and siliceous hydrogarnet. Without the formation of portlandite, which

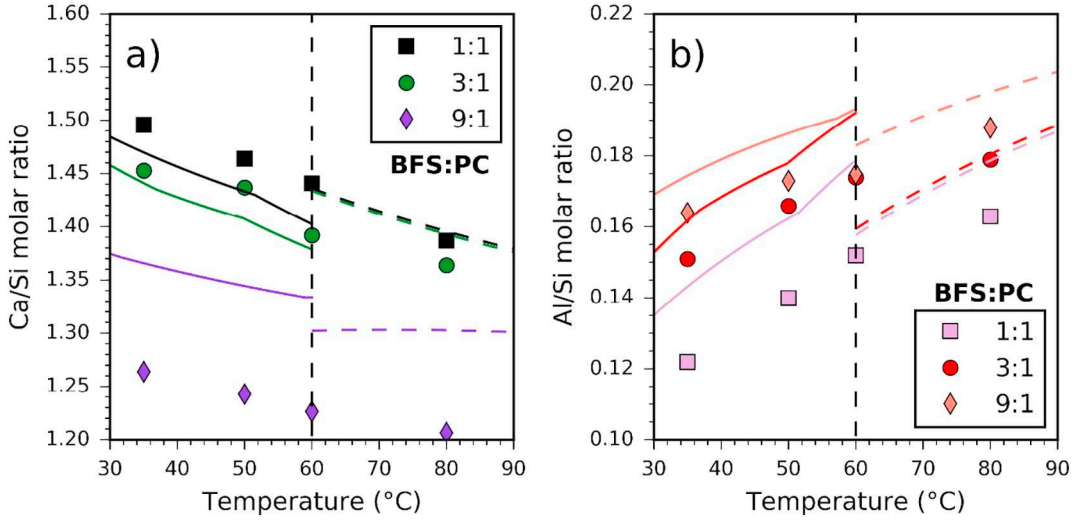

Fig. 12. Molar ratios of a) Ca/Si and b) Al/Si within C-A-S-H as a function of temperature, predicted using the two different modelling approaches (*SH* above, and *NS* below, a cutoff temperature of 60 °C in each case), as a function of the BFS:PC ratios. The symbols correspond to SEM-EDS results, while the lines represent the modelling results. The solid line represents the *NS* method and the dotted line represents the *SH* method.

was predicted in the 1:1 and 3:1 cements but not at 9:1, the C-A-S-H phase composition was influenced by the formation of the hydrogarnet phase. The hydrogarnet phase has a similar solubility to that of C-A-S-H at pH > 11.5 [36,66], so both phases co-exist in the 9:1 cement. The amount of siliceous hydrogarnet remains relatively constant throughout the *SH method* simulations for each BFS-PC ratio as a function of temperature.

The Ca/Si values within C-A-S-H were generally under-predicted in the *NS method* due to the competition with other calcium containing phases. However, the Al/Si was generally over-predicted due to the lower Gibbs energy of the 5CA and INFCA end-members (end-member model used to describe C-A-S-H phase, Table 7 [58]). This was exhibited further by the sudden increase of the Al/Si in the C-A-S-H phase once the decomposition of ettringite occurs. A combination of these two factors led to an increase in availability of calcium for higher portlandite formation observed in the 1:1 and 3:1 cements. Within the 9:1 systems, the Ca/Si was over-predicted consistently due to the lower Ca/Si end-members withdrawing the calcium from solution in place of forming portlandite.

The Ca/Si ratio in the *SH method* was generally over-predicted due to the C-A-S-H phase containing a higher calcium content when compared to siliceous hydrogarnet which was competing for calcium. Similarly, the Al/Si within C-A-S-H was reduced in the *SH method* compared to the NS method due to siliceous hydrogarnet containing a higher Al/Si ratio than the end-members used for the creation of C-A-S-H and was stable throughout the temperature range (60–90 °C), whereas phases such as ettringite were not stable across the temperature range in the *NS method* (30–60 °C).

This impact on the level of change of the Ca/Si and Al/Si at each temperature point was not explicitly observed via the SEM-EDS data, however the general trends of decreasing Ca/Si and increasing Al/Si with the increase of temperature were observed in both modelling methods and in the SEM-EDS data as exhibited in Fig. 12.

For both methods, the polymerisation of the aluminosilicate chains was well represented due to the resulting reduction of Ca/Si and increase in Al/Si in the C-A-S-H phase, with increased curing temperature. For the 1:1 and 3:1 samples, the Ca/Si was under-predicted and the Al/Si was over-predicted by up to 2.1% and 13.8% respectively. Integrating aluminium-containing end-members into C-A-S-H models has been a continual issue. Recreating aluminium end-members with lower (Al/Si = 0.1) or very high (Al/Si = 0.33) Al contents based on the additive method proposed by Kulik [67] and by Myers et al. [68] did not provide useful additions to the C-A-S-H model for the cementitious systems simulated in this study. The highly stable nature of the current end-members causes a redundancy in other end-members because they do not form in any meaningful amounts to contribute to the phase assemblage of blended cements or the chemical composition of C-A-S-H in varying environments. This is further highlighted by the results for the 9:1 cement system, which rigidly maintains a Ca/Si ratio between 1.3 and 1.37, accumulating the remaining calcium in the system that cannot reach the higher Ca concentration required to form portlandite. As a result of the C-A-S-H phase restricting the formation of portlandite, its Ca/Si ratio was over-predicted in the 9:1 system by up to 7.4%. The higher Al/Si ratio expected in the 9:1 cement resulted in greater accuracy, whereby the Al/Si was over-estimated by no more than 7.6%.

5. Conclusions

The alteration in phase assemblages in hydrated mature BFS-PC systems which are subjected to step-changes in temperature occurs relatively rapidly, and is of importance in the context of emplacement of cemented nuclear waste in a geological disposal facility. Sulphate and carbonate containing AFm and AFt type phases are not greatly affected by the increase of temperature from 35 to 50 °C after 360 days of curing at 35 °C; transferring these samples to an environment of 50 °C did not cause major phase changes. However, the higher water content phases such as ettringite and hemicarbonate become destabilised at around 60 °C. When a 360-day cured cement is transferred from 35 to 80 °C environments, a rapid transition occurs: after 3 to 7 days, the sulphate and carbonate AFm and AFt phases have been destabilised and replaced by siliceous hydrogarnet.

Thermodynamic modelling of these systems has been shown to accurately replicate the changes in phase assemblage observed when cements are transferred to higher temperature after 360 days of curing, when held at the elevated temperature for 28 days at a range of temperatures, and up to 360 days in the case of a transfer to an 80 °C environment.

The phase assemblage formed after a subsequent decrease of temperature from 80 °C to 50 °C (after 360 days at 35 °C and another 360 days at 80 °C) could be accurately predicted by a model which allowed siliceous hydrogarnet to form, although this phase needed to be suppressed in simulations of the samples which had never been heated above 60 °C. This provides further evidence that the absence of siliceous

hydrogarnet from cement phase assemblages at near-ambient or slightly elevated temperature is due to kinetic, rather than pure thermodynamic, limitations.

Description of the chemical composition of the C-A-S-H phase followed the trends observed experimentally in BFS-PC cements. The Ca/Si values were very slightly under-predicted for the 1:1 and 3:1 systems, and over-predicted in the 9:1 cement by up to 7.4%. The Al/Si ratio was over-predicted in all cements, by up to 13.8% in the worst cases. Inclusion of additional end-members with low (Al/Si = 0.1) or high Al/Si (Al/Si = 0.33) values based on the additive method did not contribute any meaningful change on the chemical composition of the C-A-S-H phase.

Understanding of how the C-A-S-H phase forms and alters with composition, and the quantity of other phase formation, is important in waste immobilisation applications as it enables prediction of how this key phase interacts with dissolved species including radionuclides. Additional studies are required to determine the effects of alkali, aluminium and groundwater leaching effects on the C-A-S-H phase, but this study has provided essential insight into the temperature effects that may influence PC-BFS blends in this safety-critical application.

Acknowledgements

D. Prentice is grateful to the National Nuclear Laboratory and EPSRC for sponsoring his PhD research studies through an iCASE Award. The participation of S.A. Bernal in this study was sponsored by EPSRC through her Early Career Fellowship (EP/R001642/1). This research was performed in part at the MIDAS Facility, at the University of Sheffield, which was established with support from the UK Department of Energy and Climate Change.

References

[1] Nuclear Decomissioning Authority, Radioactive Wastes in the UK: Summary of Data for International Reporting 2016, https://ukinventory.nda.gov.uk/wp-content/uploads/sites/18/2014/01/2016-UKRWMI-Summary-of-Data-for-International-Reporting-1.pdf, (2017).

[2] S.J. Benbow, M.O. Rivett, N. Chittenden, A.W. Herbert, S. Watson, S.J. Williams, S. Norris, Potential migration of buoyant LNAPL from Intermediate Level Waste (ILW) emplaced in a Geological Disposal Facility (GDF) for UK radioactive waste, J. Contam. Hydrol. 167 (2014) 1–22, https://doi.org/10.1016/j.jconhyd.2014.07.011.

[3] A.J. Francis, R. Cather, I.G. Crossland, Science Report Nirex Safety Assessment Research Programme: Development of the Nirex Reference Vault Backfill, Report on Current Status in 1994, (1997).

[4] R.G.W. Vasconcelos, N. Beaudoin, A. Hamilton, N.C. Hyatt, J.L. Provis, C.L. Corkhill, Characterisation of a high pH cement backfill for the geological disposal of nuclear waste: the Nirex Reference Vault Backfill, Appl. Geochem. 89 (2017) 180–189, https://doi.org/10.1016/j.apgeochem.2017.11.007.

[5] M. Atkins, F.P. Glasser, Application of Portland cement-based materials to radioactive waste immobilization, Waste Manag. 12 (1992) 105–131, https://doi.org/10.1016/0956-053X(92)90044-J.

[6] M. Moranville-Regourd, Cements made from blastfurnace slag, in: P.C. Hewlett (Ed.), Lea's Chemistry of Cement and Concrete, 4th ed., 2003, pp. 637–678, , https://doi.org/10.1016/B978-075066256-7/50023-0.

[7] F.P. Glasser, Progress in the immobilization of radioactive wastes in cement, Cem. Concr. Res. 22 (1992) 201–216, https://doi.org/10.1016/0008-8846(92)90058-4.

[8] J.H. Sharp, J. Hill, N.B. Milestone, E.W. Miller, Cementitious systems for encapsulation of intermediate level waste, Proc. ICEM 2003 9th Int. Conf. Radioact. Waste Manag. Environ. Remediat, 2003, pp. 1–10, , https://doi.org/10.1115/ICEM2003-4554.

[9] N.C. Collier, N.B. Milestone, The encapsulation of $Mg(OH)_2$ sludge in composite cement, Cem. Concr. Res. 40 (2010) 452–459, https://doi.org/10.1016/j.cemconres.2009.10.007.

[10] M.I. Ojovan, W.E. Lee, An Introduction to Nuclear Waste Immobilisation, Elsevier, Amsterdam, 2006, https://doi.org/10.1016/S1369-7021(06)71394-3.

[11] C.A. Utton, M. Hayes, J. Hill, N.B. Milestone, J.H. Sharp, Effect of temperatures up to 90 °C on the early hydration of Portland-blastfurnace slag cements, J. Am. Ceram. Soc. 91 (2008) 948–954, https://doi.org/10.1111/j.1551-2916.2007.02124.x.

[12] F.M.I. Hunter, B.T. Swift, An Assessment of the Generation of GDF-derived Gas Using the 2007 Derived Inventory, AMEC, 2013.

[13] H. Godfrey, G. Cann, Effect of Chloride on Magnox Corrosion With Respect to Carbon-14 Release Post Closure, NNL, Risley, 2015.

[14] S.C. Boden, Nirex Vault Environment Feasibility Study: Summary Report, NNC Ltd., 2002.

[15] NDA, Geological Disposal: Guidance on the Application of the Waste Package Specifications for Unshielded Waste Packages, Oxford, 2014.

[16] B. Lothenbach, T. Matschei, G. Möschner, F.P. Glasser, Thermodynamic modelling of the effect of temperature on the hydration and porosity of Portland cement, Cem. Concr. Res. 38 (2008) 1–18, https://doi.org/10.1016/j.cemconres.2007.08.017.

[17] J.J. Thomas, D. Rothstein, H.M. Jennings, B.J. Christensen, Effect of hydration temperature on the solubility behavior of Ca-, S-, Al-, and Si-bearing solid phases in Portland cement pastes, Cem. Concr. Res. 33 (2003) 2037–2047, https://doi.org/10.1016/S0008-8846(03)00224-2.

[18] T. Matschei, B. Lothenbach, F.P. Glasser, Thermodynamic properties of Portland cement hydrates in the system $CaO\text{-}Al_2O_3\text{-}SiO_2\text{-}CaSO_4\text{-}CaCO_3\text{-}H_2O$, Cem. Concr. Res. 37 (2007) 1379–1410, https://doi.org/10.1016/j.cemconres.2007.06.002.

[19] T. Matschei, F.P. Glasser, Temperature dependence, 0 to 40 °C, of the mineralogy of Portland cement paste in the presence of calcium carbonate, Cem. Concr. Res. 40 (2010) 763–777, https://doi.org/10.1016/j.cemconres.2009.11.010.

[20] F.P. Glasser, J. Pedersen, K. Goldthorpe, M. Atkins, Solubility reactions of cement components with NaCl solutions: I. $Ca(OH)_2$ and C-S-H, Adv. Cem. Res. 17 (2005) 57–64, https://doi.org/10.1680/adcr.2005.17.2.57.

[21] S. Martínez-Ramírez, M. Frías, The effect of curing temperature on white cement hydration, Constr. Build. Mater. 23 (2009) 1344–1348, https://doi.org/10.1016/j.conbuildmat.2008.07.012.

[22] S. Bahafid, S. Ghabezloo, M. Duc, P. Faure, J. Sulem, Effect of the hydration temperature on the microstructure of Class G cement: C-S-H composition and density, Cem. Concr. Res. 95 (2017) 270–281, https://doi.org/10.1016/j.cemconres.2017.02.008.

[23] J.I. Escalante-García, J.H. Sharp, The chemical composition and microstructure of hydration products in blended cements, Cem. Concr. Compos. 26 (2004) 967–976, https://doi.org/10.1016/j.cemconcomp.2004.02.036.

[24] F. Deschner, B. Lothenbach, F. Winnefeld, J. Neubauer, Effect of temperature on the hydration of Portland cement blended with siliceous fly ash, Cem. Concr. Res. 52 (2013) 169–181, https://doi.org/10.1016/j.cemconres.2013.07.006.

[25] C.C. Castellano, V.L. Bonavetti, H.A. Donza, E.F. Irassar, The effect of w/b and temperature on the hydration and strength of blastfurnace slag cements, Constr. Build. Mater. 111 (2016) 679–688, https://doi.org/10.1016/j.conbuildmat.2015.11.001.

[26] R.J. Myers, S.A. Bernal, J.D. Gehman, J.S.J. Van Deventer, J.L. Provis, The role of Al in cross-linking of alkali-activated slag cements, J. Am. Ceram. Soc. 98 (2015) 996–1004, https://doi.org/10.1111/jace.13360.

[27] R.J. Myers, E. L'Hôpital, J.L. Provis, B. Lothenbach, Effect of temperature and aluminium on calcium (alumino)silicate hydrate chemistry under equilibrium conditions, Cem. Concr. Res. 68 (2015) 83–93, https://doi.org/10.1016/j.cemconres.2014.10.015.

[28] T.T.H. Bach, C. Cau Dit Coumes, I. Pochard, C. Mercier, B. Revel, A. Nonat, Influence of temperature on the hydration products of low pH cements, Cem. Concr. Res. 42 (2012) 805–817, https://doi.org/10.1016/j.cemconres.2012.03.009.

[29] J.I. Escalante-García, J.H. Sharp, Effect of temperature on the hydration of the main clinker phases in Portland cements: part I, neat cements, Cem. Concr. Res. 28 (1998) 1245–1257, https://doi.org/10.1016/S0008-8846(98)00115-X.

[30] J.I. Escalante-García, J.H. Sharp, Effect of temperature on the hydration of the main clinker phases in Portland cements: part II, blended cements, Cem. Concr. Res. 28 (1998) 1245–1257, https://doi.org/10.1016/S0008-8846(98)00115-X.

[31] J.I. Escalante, L.Y.Y. Gómez, K.K. Johal, G. Mendoza, H. Mancha, J. Méndez, Reactivity of blast-furnace slag in Portland cement blends hydrated under different conditions, Cem. Concr. Res. 31 (2001) 1403–1409, https://doi.org/10.1016/S0008-8846(01)00587-7.

[32] D. Damidot, B. Lothenbach, D. Herfort, F.P. Glasser, Thermodynamics and cement science, Cem. Concr. Res. 41 (2011) 679–695, https://doi.org/10.1016/j.cemconres.2011.03.018.

[33] B.A. Clark, P.W. Brown, The formation of calcium sulfoaluminate hydrate compounds: part I, Cem. Concr. Res. 29 (1999) 1943–1948, https://doi.org/10.1016/S0008-8846(99)00200-8.

[34] B.A. Clark, P.W. Brown, The formation of calcium sulfoaluminate hydrate compounds: part II, Cem. Concr. Res. 30 (2000) 233–240, https://doi.org/10.1016/S0008-8846(99)00234-3.

[35] M.U. Okoronkwo, F.P. Glasser, Compatibility of hydrogarnet, $Ca_3Al_2(SiO_4)_x(OH)_{4(3-x)}$, with sulfate and carbonate-bearing cement phases: 5–85 °C, Cem. Concr. Res. 83 (2016) 86–96, https://doi.org/10.1016/j.cemconres.2016.01.013.

[36] B.Z. Dilnesa, B. Lothenbach, G. Renaudin, A. Wichser, D.A. Kulik, Synthesis and characterization of hydrogarnet $Ca_3(Al_xFe_{1-x})_2(SiO_4)_y(OH)_{4(3-y)}$, Cem. Concr. Res. 59 (2014) 96–111, https://doi.org/10.1016/j.cemconres.2014.02.001.

[37] K. Kyritsis, N. Meller, C. Hall, Chemistry and morphology of hydrogarnets formed in cement-based CASH hydroceramics cured at 200° to 350 °C, J. Am. Ceram. Soc. 92 (2009) 1105–1111, https://doi.org/10.1111/j.1551-2916.2009.02958.x.

[38] I.G. Richardson, Clarification of possible ordered distributions of trivalent cations in layered double hydroxides and an explanation for the observed variation in the lower solid-solution limit, Acta Crystallogr. Sect. B Struct. Sci. Cryst. Eng. Mater. 69 (2013) 629–633, https://doi.org/10.1107/S2052519213027905.

[39] B. Lothenbach, K.L. Scrivener, R.D. Hooton, Supplementary cementitious materials, Cem. Concr. Res. 41 (2011) 1244–1256, https://doi.org/10.1016/j.cemconres.2010.12.001.

[40] K.L. Scrivener, A. Nonat, Hydration of cementitious materials, present and future, Cem. Concr. Res. 41 (2011) 651–665, https://doi.org/10.1016/j.cemconres.2011.03.026.

[41] R.J. Myers, B. Lothenbach, S.A. Bernal, J.L. Provis, Thermodynamic modelling of alkali-activated slag cements, Appl. Geochem. 61 (2015) 233–247, https://doi.org/

10.1016/j.apgeochem.2015.06.006.
[42] I. Ismail, S.A. Bernal, J.L. Provis, S. Hamdan, J.S.J. Van Deventer, Drying-induced changes in the structure of alkali-activated pastes, J. Mater. Sci. 48 (2013) 3566–3577, https://doi.org/10.1007/s10853-013-7152-9.
[43] K.L. Scrivener, A. Bazzoni, B. Mota, J.E. Rossen, Electron microscopy, in: K.L. Scrivener, R. Snellings, B. Lothenbach (Eds.), A Pract. Guid. to Microstruct. Anal. Cem. Mater, 1st ed., CRC Press, 2016, , https://doi.org/10.1007/978-1-62703-776-1.
[44] J.E. Rossen, K.L. Scrivener, Optimization of SEM-EDS to determine the C–A–S–H composition in matured cement paste samples, Mater. Charact. 123 (2017) 294–306, https://doi.org/10.1016/j.matchar.2016.11.041.
[45] P.T. Durdziński, M. Ben Haha, M. Zajac, K.L. Scrivener, Phase assemblage of composite cements, Cem. Concr. Res. 99 (2017) 172–182, https://doi.org/10.1016/j.cemconres.2017.05.009.
[46] D.P. Prentice, S.A. Bernal, M. Bankhead, M. Hayes, J.L. Provis, Phase evolution of slag-rich cementitious grouts for immobilisation of nuclear wastes, Adv. Cem. Res. 30 (2018) 345–360, https://doi.org/10.1680/jadcr.17.00198.
[47] D.A. Kulik, T. Wagner, S.V. Dmytrieva, G. Kosakowski, F.F. Hingerl, K.V. Chudnenko, U.R. Berner, GEM-Selektor geochemical modeling package: revised algorithm and GEMS3K numerical kernel for coupled simulation codes, Comput. Geosci. 17 (2013) 1–24, https://doi.org/10.1007/s10596-012-9310-6.
[48] T. Wagner, D.A. Kulik, F.F. Hingerl, S.V. Dmytrievava, Gem-selektor geochemical modeling package: TSolMod library and data interface for multicomponent phase models, Can. Mineral. 50 (2012) 1173–1195, https://doi.org/10.3749/canmin.50.5.1173.
[49] H.C. Helgeson, D.H. Kirkham, G.C. Flowers, Theoretical prediction of the thermodynamic behavior of aqueous electrolytes by high pressures and temperatures IV; calculation of activity coefficients, osmotic coefficients and apparent molal & standard relative partial molal properties to 600 °C & 5 kB, Am. J. Sci. 281 (1981) 1249–1516, https://doi.org/10.2475/ajs.281.10.1249.
[50] A. Vollpracht, B. Lothenbach, R. Snellings, J. Haufe, The pore solution of blended cements: a review, Mater. Struct. 49 (2015) 3341–3367, https://doi.org/10.1617/s11527-015-0724-1.
[51] M. Regourd, Structure and behaviour of slag Portland cement hydrates, Proc. 7th Int. Congr. Chem. Cem. Paris, Fr. I, 1980 (III-2/10-26).
[52] J.J. Thomas, H.M. Jennings, A colloidal interpretation of chemical aging of the C-S-H gel and its effects on the properties of cement paste, Cem. Concr. Res. 36 (2006) 30–38, https://doi.org/10.1016/j.cemconres.2004.10.022.
[53] X. Cong, R.J. Kirkpatrick, Effects of the temperature and relative humidity on the structure of CSH gel, Cem. Concr. Res. 25 (1995) 1237–1245, https://doi.org/10.1016/0008-8846(95)00116-T.
[54] X. Ke, S.A. Bernal, J.L. Provis, Uptake of chloride and carbonate by Mg-Al and Ca-Al layered double hydroxides in simulated pore solutions of alkali-activated slag cement, Cem. Concr. Res. 100 (2017) 1–13, https://doi.org/10.1016/j.cemconres.2017.05.015.
[55] G.D. Miron, T. Wagner, D.A. Kulik, B. Lothenbach, An internally consistent thermodynamic dataset for aqueous species in the system Ca-Mg-Na-K-Al-Si-O-H-C-Cl to 800 °C and 5 KBAR, Am. J. Sci. 317 (2017) 755–806, https://doi.org/10.2475/07.2017.01.
[56] J.M. Rivas Mercury, P. Pena, A.H. De Aza, X. Turrillas, I. Sobrados, J. Sanz, Solid-state ^{27}Al and ^{29}Si NMR investigations on Si-substituted hydrogarnets, Acta Mater. 55 (2007) 1183–1191, https://doi.org/10.1016/j.actamat.2006.09.032.
[57] I.G. Richardson, S. Li, Composition and structure of an 18-year-old 5M KOH-activated ground granulated blast-furnace slag paste, Constr. Build. Mater. 168 (2018) 404–411, https://doi.org/10.1016/j.conbuildmat.2018.02.034.
[58] D.P. Prentice, B. Walkley, S.A. Bernal, M. Bankhead, M. Hayes, J.L. Provis, Compositional analysis of Ca-Si-Al-OH phases of BFS-PC exposed to 35, 50, 60 and 80 °C and accompanying thermodynamic data, Cem. Concr. Res. - Data Br. (2018) (Submitted).
[59] O. Burciaga-Díaz, L.Y. Gómez-Zamorano, J.I. Escalante-García, Influence of the long term curing temperature on the hydration of alkaline binders of blast furnace slag-metakaolin, Constr. Build. Mater. 113 (2016) 917–926, https://doi.org/10.1016/j.conbuildmat.2016.03.111.
[60] B.Z. Dilnesa, E. Wieland, B. Lothenbach, R. Dähn, K.L. Scrivener, Fe-containing phases in hydrated cements, Cem. Concr. Res. 58 (2014) 45–55, https://doi.org/10.1016/j.cemconres.2013.12.012.
[61] R. Taylor, I.G. Richardson, R.M.D. Brydson, Composition and microstructure of 20-year-old ordinary Portland cement–ground granulated blast-furnace slag blends containing 0 to 100% slag, Cem. Concr. Res. 40 (2010) 971–983, https://doi.org/10.1016/j.cemconres.2010.02.012.
[62] S.Y. Hong, F.P. Glasser, Alkali binding in cement pastes. Part I: the C-S-H phase, Cem. Concr. Res. 29 (1999) 1893–1903, https://doi.org/10.1016/S0008-8846(99)00187-8.
[63] S.Y. Hong, F.P. Glasser, Alkali sorption by C-S-H and C-A-S-H gels: part II. Role of alumina, Cem. Concr. Res. 32 (2002) 1101–1111, https://doi.org/10.1016/S0008-8846(02)00753-6.
[64] L. Divet, R. Randriambololona, Delayed ettringite formation: the effect of temperature and basicity on the interaction of sulphate and C-S-H phase, Cem. Concr. Res. 28 (1997) 357–363 (doi: 0008-8846/98).
[65] T. Matschei, B. Lothenbach, F.P. Glasser, The AFm phase in Portland cement, Cem. Concr. Res. 37 (2007) 118–130, https://doi.org/10.1016/j.cemconres.2006.10.010.
[66] E. L'Hôpital, B. Lothenbach, K. Scrivener, D.A. Kulik, Alkali uptake in calcium alumina silicate hydrate (C-A-S-H), Cem. Concr. Res. 85 (2016) 122–136, https://doi.org/10.1016/j.cemconres.2016.03.009.
[67] D.A. Kulik, Improving the structural consistency of C-S-H solid solution thermodynamic models, Cem. Concr. Res. 41 (2011) 477–495, https://doi.org/10.1016/j.cemconres.2011.01.012.
[68] R.J. Myers, S.A. Bernal, J.L. Provis, A thermodynamic model for C-(N-)A-S-H gel: CNASH_ss. Derivation and validation, Cem. Concr. Res. 66 (2014) 27–47, https://doi.org/10.1016/j.cemconres.2014.07.005.